

# Automatic segmentation and 3D reconstruction of intravascular ultrasound images for a fast preliminar evaluation of vessel pathologies

Roberto Sanz-Requena<sup>a</sup>, David Moratal<sup>a,\*</sup>, Diego Ramón García-Sánchez<sup>a</sup>,  
Vicente Bodí<sup>b</sup>, José Joaquín Rieta<sup>a</sup>, Juan Manuel Sanchis<sup>a</sup>

<sup>a</sup> *Electronics Engineering Department, Universitat Politècnica de València, Valencia, Spain*

<sup>b</sup> *Cardiology Department, Hospital Clínico Universitario, Valencia, Spain*

Received 15 August 2005; received in revised form 17 February 2006; accepted 6 November 2006

## Abstract

Intravascular ultrasound (IVUS) imaging is used along with X-ray coronary angiography to detect vessel pathologies. Manual analysis of IVUS images is slow and time-consuming and it is not feasible for clinical purposes. A semi-automated method is proposed to generate 3D reconstructions from IVUS video sequences, so that a fast diagnose can be easily done, quantifying plaque length and severity as well as plaque volume of the vessels under study. The methodology described in this work has four steps: a pre-processing of IVUS images, a segmentation of media–adventitia contour, a detection of intima and plaque and a 3D reconstruction of the vessel. Preprocessing is intended to remove noise from the images without blurring the edges. Segmentation of media–adventitia contour is achieved using active contours (snakes). In particular, we use the gradient vector flow (GVF) as external force for the snakes. The detection of lumen border is obtained taking into account gray-level information of the inner part of the previously detected contours. A knowledge-based approach is used to determine which level of gray corresponds statistically to the different regions of interest: intima, plaque and lumen. The catheter region is automatically discarded. An estimate of plaque type is also given. Finally, 3D reconstruction of all detected regions is made.

The suitability of this methodology has been verified for the analysis and visualization of plaque length, stenosis severity, automatic detection of the most problematic regions, calculus of plaque volumes and a preliminary estimation of plaque type obtaining for automatic measures of lumen and vessel area an average error smaller than 1 mm<sup>2</sup> (equivalent approximately to 10% of the average measure), for calculus of plaque and lumen volume errors smaller than 0.5 mm<sup>3</sup> (equivalent approximately to 20% of the average measure) and for plaque type estimates a mismatch of less than 8% in the analysed frames.

© 2006 Elsevier Ltd. All rights reserved.

**Keywords:** Intravascular ultrasound; 3D reconstruction; Plaque estimation; Segmentation method

## 1. Introduction

IVUS (intravascular ultrasound) technology appears in the 1970s [1,2] as an aid tool for endovascular surgery. At that time angiography only offered a limited point of view of vascular pathologies, dismissing the amount of information that axial sections of a blood vessel can provide, i.e. plaque composition or plaque thickness. Looking at their characteristics, angiography and IVUS are complementary technologies, while IVUS offers an internal vision of the vessel, angiography defines the situation of that vessel in the body [3,4].

IVUS technique consists in analyzing a series of video images recorded with an ultrasound transducer. This transducer is attached to a catheter which is inserted into the vessel. The images are recorded while the catheter is being pulled out [1]. Manual analysis of these images is very slow and it doesn't provide a global vision of the vessel under study. Therefore it is necessary to use automatic or semi-automatic methods to speed up the analysis process. These methods are normally based in computing algorithms whose aim is to detect the regions of interest in each video frame, usually the media–adventitia contour and the intima/plaque-lumen contour as shown in Fig. 1. Several studies on how to solve this problem have been carried out [5–10]. Most of them are based in the minimization of cost functions applied to the regions of interest. When a minimum is reached it is supposed that the border has been located. Once the

\* Corresponding author. Tel.: +34 962849441.  
E-mail address: [dmoratal@eln.upv.es](mailto:dmoratal@eln.upv.es) (D. Moratal).

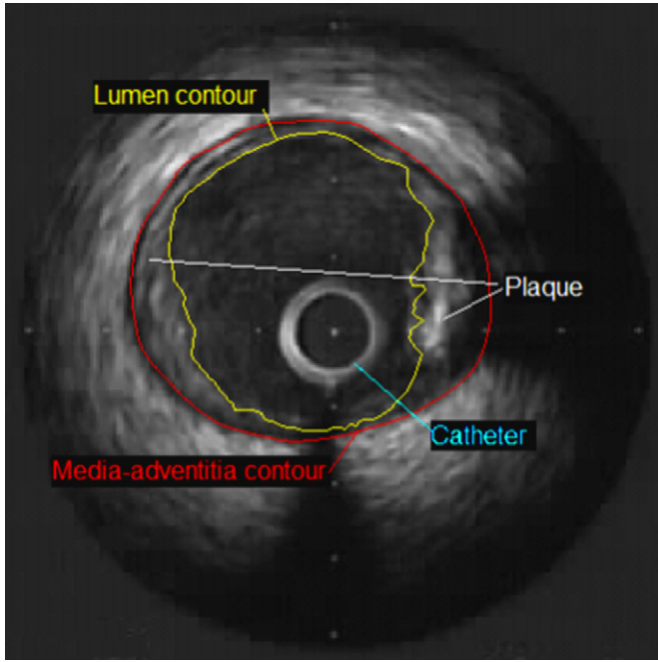


Fig. 1. Lumen and media–adventitia contour automatically detected for an intravascular ultrasound image. The catheter and the plaque are also pointed out—the later will be automatically estimated.

regions of interest have been detected the next step is the three-dimensional reconstruction of the vessel. The specialist can use this reconstruction to take measures of area, volume and length, as well as to get a first estimation of plaque severity and a fast access to any region of interest.

The proposed method consists of five steps: acquiring a video frame, preprocessing of the image using a median filter and discrimination of non-interest regions, detection of the regions of interest using active contours models [9] for the media–adventitia border and a gray-level knowledge-based approach [10] for the lumen border and, finally, a three-dimensional reconstruction. Fig. 2 shows a diagram with the whole process.

## 2. Materials and methods

The IVUS images were acquired using a Clearview Ultra (Boston Scientific Corp., Natick, MA, USA) with a catheter model Atlantis. The ultrasound frequency was 40 MHz and the catheter pull-out speed was 0.5 mm/s. Initially the IVUS video was recorded on a VHS tape. To digitize the video sequence a Pinnacle card was used generating an AVI sequence encoded with PIM1 codec with a frame rate of 25 fps (frames per second) and a resolution of  $352 \times 288$  pixels, equivalent to 26 pixels per millimetre.

All the methodology was implemented in MATLAB R13 (The Mathworks Inc., Natick, MA, USA).

### 2.1. Preprocessing

The first step of our methodology consisted in determining the image zones where our regions of interest may be choosing a squared region of interest (ROI) as shown in Fig. 3.

IVUS images are quite noisy, so a noise reduction filtering was considered. Because next step is border detection, it was necessary for the filter to be noise-reductor and edge-enhancer. Three different types of filters were studied: Gaussian filter, anisotropic filter (using Perona–Malik algorithm [11]) and median filter.

A median filter of size 7 was finally used because its good results for noise reduction and edge enhancement and also because it was relatively fast in comparison to the other evaluated filters. Fig. 4 shows a comparison of the three types of filter evaluated for our IVUS images.

### 2.2. Segmentation: media–adventitia contour detection

Active contour models, or snakes [9,12], were used to detect the media–adventitia contour. In these models the energy function to minimize is

$$E_{\text{snake}}(V) = \sum_{i=1}^n E_{\text{int}}(v_i) + \kappa E_{\text{ext}}(v_i, I) \quad (1)$$

where  $V = [v_1, \dots, v_n]$  defines the contour points,  $v_i = (x_i, y_i)$ ,  $x_i$  and  $y_i$  are the coordinates of the contour,  $\kappa$  is a weight factor,  $E_{\text{snake}}$  the total energy associated to the snake,  $E_{\text{int}}$  the energy associated to the contour in itself and  $E_{\text{ext}}$  is the energy associated to both the contour and the characteristics of the image  $I$ .

The internal energy is determined from the characteristics of the present contour. This means that an initial contour must be manually defined prior to let the contour deform to search the minimum energy function. For the rest of frames the previous contour was taken as initial contour for the current frame. The snake deforming algorithm uses a number of parameters which determines how the snake will internally behave, i.e. its elasticity, rigidity, viscosity and pressure force weight, without considering yet the image characteristics.

If  $V$  represents the curve, then internal energy can be written as

$$E_{\text{int}}(V) = \sum_{i=1}^n \alpha |V'(v_i)|^2 + \beta |V''(v_i)|^2 \quad (2)$$

where  $V'(v_i)$  and  $V''(v_i)$  represent the first and second derivative, respectively, and  $\alpha$  (elasticity) and  $\beta$  (rigidity) are weighting parameters.

Pressure force weight can be expressed as

$$F = k\hat{a}(V) \quad (3)$$

where  $k$  is the weighting factor and  $\hat{a}(V)$  is the normal unitary vector to the curve at any point  $v_i$ . The sign of  $k$  determines whether the curve tends to inflate or deflate, following a balloon model.

Viscosity is used in the iterative implementation as a weight to control how fast the curve can deform between iterations:

$$V_i(v_i) = f(\gamma V_{i-1}(v_i), E_{\text{ext}}) \quad (4)$$

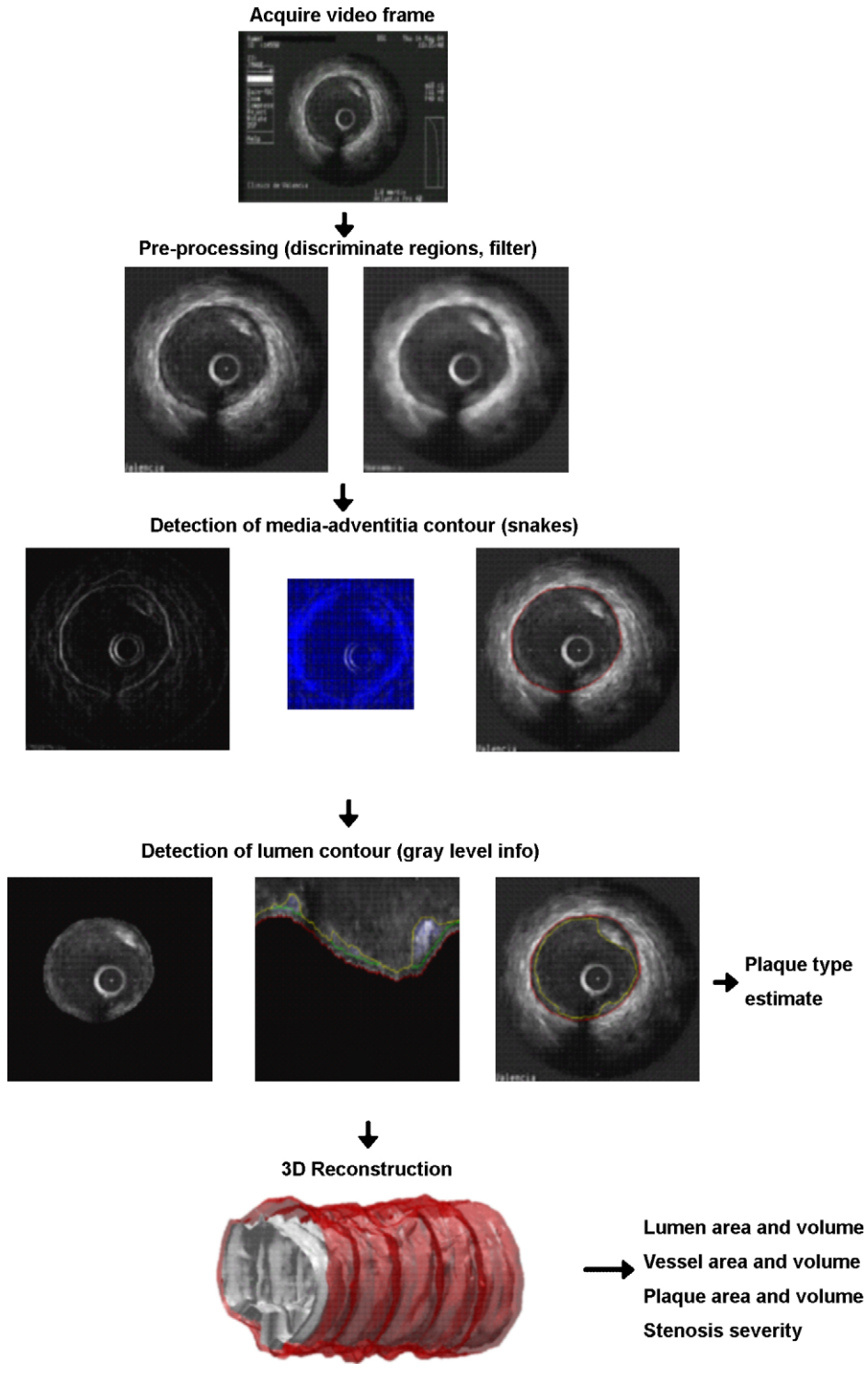


Fig. 2. Diagram with the method steps.

where  $V_t(v_i)$  and  $V_{t-1}(v_i)$  are the curve in the present iteration and the previous one, respectively,  $\gamma$  represents viscosity and  $E_{ext}$  is the external energy.

The external energy is determined from the characteristics of the image. In our method, GVF (gradient vector flow) [9] was used as external energy. The GVF algorithm generates a force field from the diffusion of the gradient vector field of

the image (see Fig. 5) where any particle, i.e. a point of the deforming contour, is pulled towards the strongest edge through a path known as streamline. The catheter region is automatically detected and discarded as it always occupies the same region of the image and it can be ignored with a simple rounded mask which cancels the gradient vector field. The input used for the GVF algorithm was not the filtered image, but an edge map of

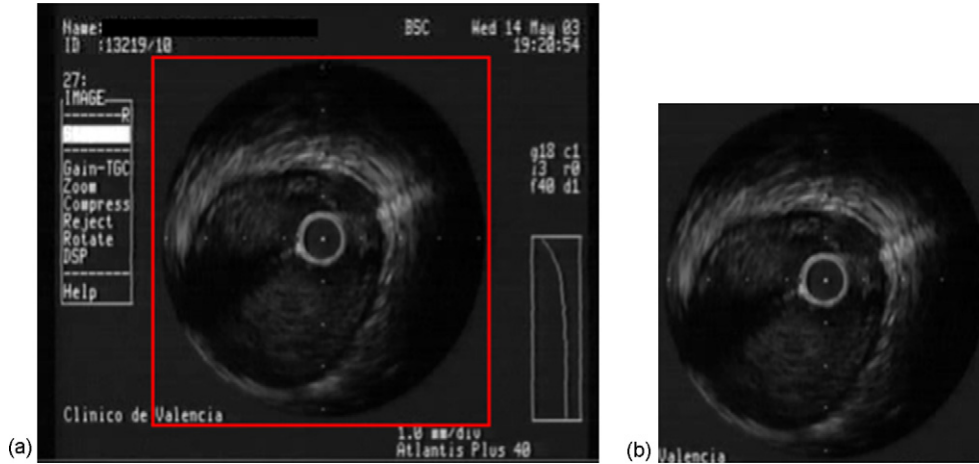


Fig. 3. (a) Original video frame. The red square marks the selected ROI (region of interest). (b) Selected ROI extracted from the original video frame. This permits a faster analysis of the image as well as a reduction of the computational burden associated to the methodology.

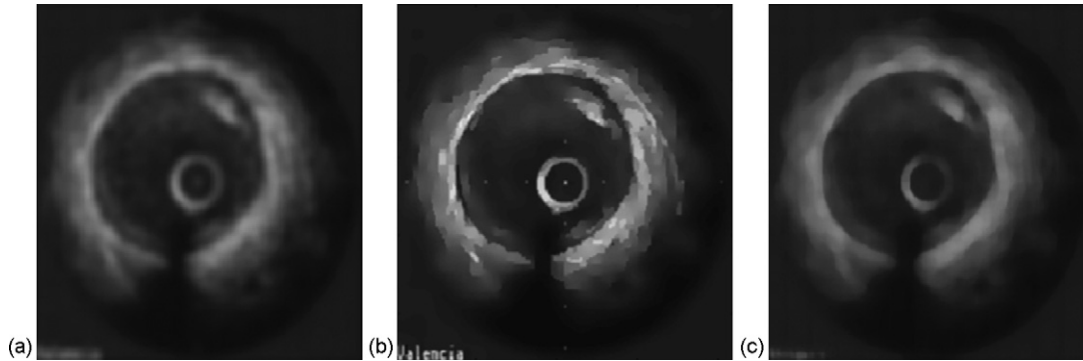


Fig. 4. Comparison of three different types of filter for our IVUS images: (a) Gaussian filter, (b) anisotropic filter and (c) median filter. It can be seen that the Gaussian filter (a) blurs the edges while both the anisotropic (b) and the median filter (c) enhance them.

it. This edge map was obtained as a combination of a Canny binary edge map and a gray-level edge map (the explanation on these maps can be found in the image processing literature, cf. [13]) calculated from the image gradient as can be observed in Fig. 6.

To minimize the energy function (1), the curve  $V$  must satisfy the Euler equation:

$$\alpha V'' - \beta V'''' - \nabla E_{\text{ext}} = 0 \tag{5}$$

In the GVF algorithm,  $-\nabla E_{\text{ext}}$  is named  $v(v_i)$ , which is the vector field that satisfies the Euler equation:

$$\mu \nabla^2 v - (v - \nabla f) |\nabla f|^2 = 0 \tag{6}$$

where  $\mu$  is a regularization parameter set according to the amount of noise in the image (more noise, higher  $\mu$ ) and  $f$  is the edge map of the image, which in our case is

$$f(x, y) = |\nabla [H_m(x, y) \otimes I(x, y)]| \tag{7}$$

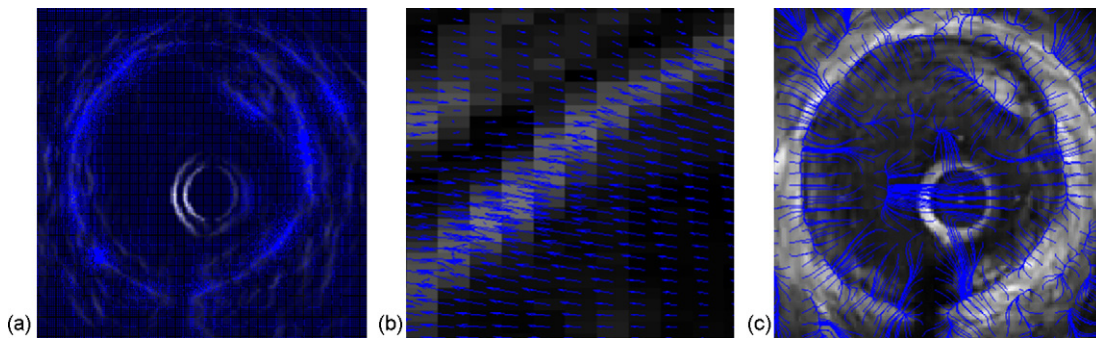


Fig. 5. (a) GVF, (b) GVF zoom of one border of interest and (c) streamlines. GVF images are shown as vector fields over the image, the size of the arrows determines the strength of the vector field in that point. Both GVF and streamlines show how the curve would be driven towards the image contours. The catheter region has been discriminated for the GVF generation.

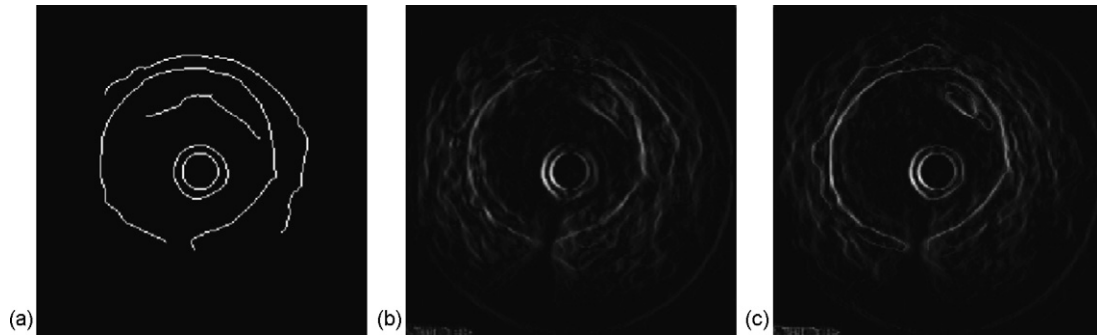


Fig. 6. (a) Canny binary edge map, (b) gray-scale edge map and (c) final edge map. We combine in (c) both edge maps (a) and (b) as an input to the GVF detection algorithm, so that both contribute to mark the borders of interest. The Canny binary edge map provides the detection of the strongest borders, while the gray-scale edge map based on the gradient of the image provides information of borders all through the image surface.

where  $H_m(x,y)$  is the median filter and  $I(x,y)$  is the original image.

The snake deforming algorithm uses the GVF ( $v$ ) to adapt the initial contour to the contour of the new image. Another parameter, the external force weight (named  $\kappa$  in (1)), determines the speed at which the initial contour is attracted to the regions defined by the GVF.

Summarizing, the snake deforming algorithm parameters are the following ones:

- alpha (elasticity) determines how rounded the curve will be (higher values mean rounder shapes);
- beta (rigidity) controls how fast the curve changes in case there's a sudden change in the contour;
- gamma (viscosity) represents the capacity of the curve to adapt to the movement of the contour across the image;
- pressure can be positive (meaning that the curve tends to inflate) or negative (then it tends to shrink);
- kappa (external force) determines the weight of the external force, that is, the importance of the information of the image; the more iterations the slower the process but the more accurate the contour will be.

And for our media–adventitia contour detection procedure we choose alpha = 80, beta = 50, gamma = 10, pressure = 0.1, kappa = 20 and iterations = 30 for the interactive method and 100–300 for our automatic algorithm.

Although our effort was intended to provide an automatic method where only the first contour should be manually specified, the characteristics of IVUS video sequences make it unfeasible to trust such an almost automated method. In IVUS images the presence of plaque produces important changes in the ultrasonic image, such as sudden shadows masking the regions of interest or the presence of artifacts and their wave reflections, which make it difficult for the contour to adapt. The catheter movement is also another important handicap because it did not allow the initial contour to adapt progressively to the desired new contour. When these situations appeared the results of our automatic method were that the initial contour adapted progressively to secondary contours which had not been completely removed by the filters.

Three possible solutions were thought to overcome the above problems:

- a correlation condition between consecutive frames was proposed to detect which images would need another manual contour definition, in this case the ones with low values of correlation, meaning that there were important changes between images;
- a periodical pause was also considered so that every certain number of images a new contour could be manually introduced;
- finally a dynamic change of the snake parameters based also on correlation values was also proposed to keep the method as automatic as possible.

The former solutions, which we called interactive, proved to be accurate but obviously less practical, while the third solution (referred here as automatic) required many more iterations for

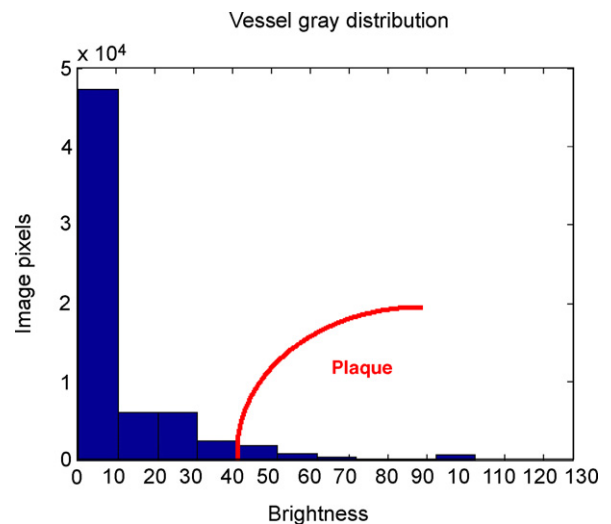


Fig. 7. Histogram of the distribution of gray shades (range 0–255) after applying ROI masks (see Fig. 8) in a random IVUS image with presence of plaque. Plaque region corresponds to those pixels whose brightness is above the range of 40–50. This threshold was chosen after analysis of the sequences by our expert observer, in which he randomly chose several plaque points on the images.

Table 1  
Lumen and vessel area results, comparing those obtained by our methods with those obtained by the manual method

	Method using interactivity (correlation stop criterium < 0.94, manual contour definition every 20 frames)		Automatic method (only first contour defined manually)	
	Lumen area	Vessel area	Lumen area	Vessel area
Average error percentages (%)	11.09	4.98	10.95	7.27
Average error (mm <sup>2</sup> )	±0.94	±0.64	±0.99	±0.9

Percentage error shows the impact of the average error on the average measure taken manually, while the average error is simply the difference between both measures, manual and interactive/automatic. The average values show that both methods are more accurate in calculating vessel area than in calculating lumen area because plaque detection, i.e. lumen area calculus, may be mistaken when there's soft plaque, as this can be easily confused with lumen.

similar results and was more dependent on the quality of the videos, as the contour is left to adapt progressively “on its own”. In the results presented in this paper we have used and compared the interactive method (as a combination of the first and second solutions explained above) and the automatic one.

However, in spite of all the improvements mentioned above, snakes have a strong limitation when it comes to initialization in IVUS images. Initial contour must be defined close to the desired contour, so that image noise and artifacts do not interfere in the first adaptation.

### 2.3. Plaque detection

Once the media–adventitia contour was obtained it was used as a mask on the video image to discriminate the internal region of the vessel: intima, plaque, lumen and catheter. With the new region of interest properly isolated, a polar coordinates transformation was then applied for an easier detection of the gray levels. On this transformation the catheter region was also dismissed and then a search algorithm was used to distinguish between lumen and plaque. An statistical study showed us that the inten-

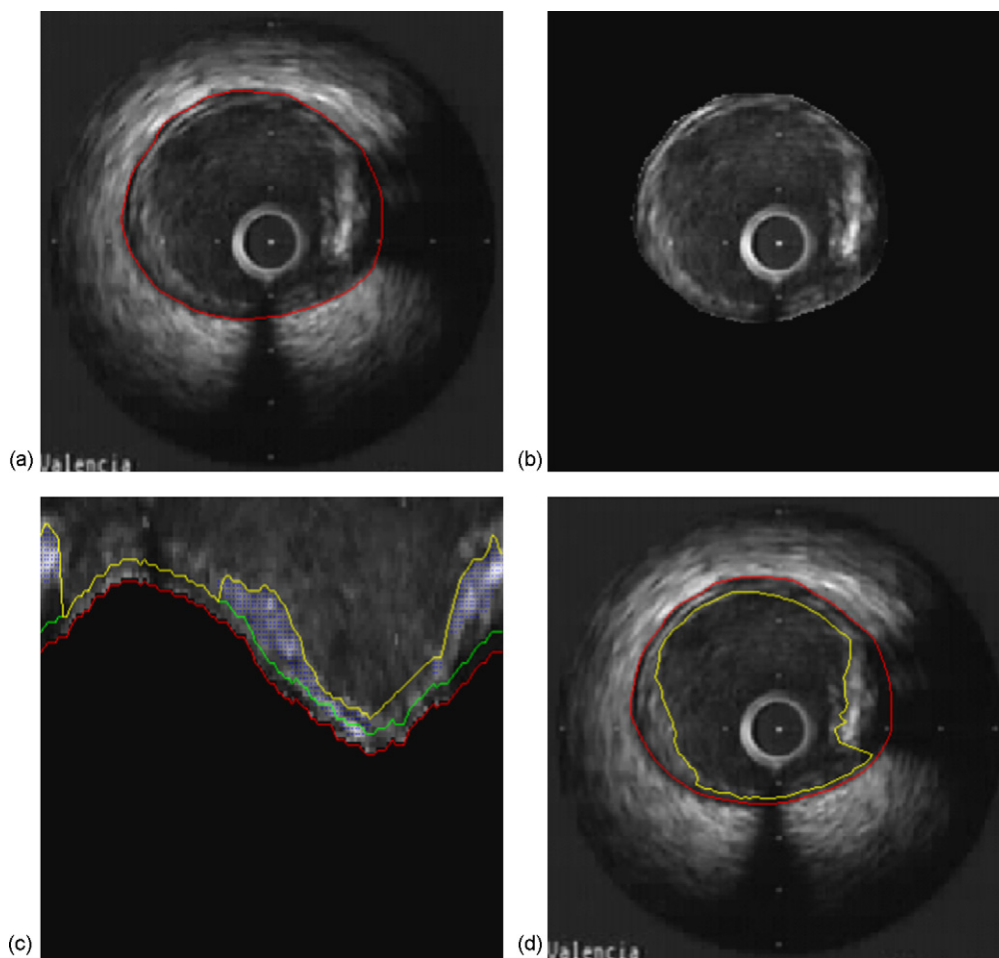


Fig. 8. (a) Media–adventitia on original image, (b) media–adventitia mask, (c) polar transformation and plaque detection results, (d) Cartesian transformation with final results. It can be seen in (c) that the plaque pixels are always “attached” or near the media–adventitia contour (red). The green line in (c) is an estimate of the intima. In case there is no plaque, the lumen border and the intima border are the same.

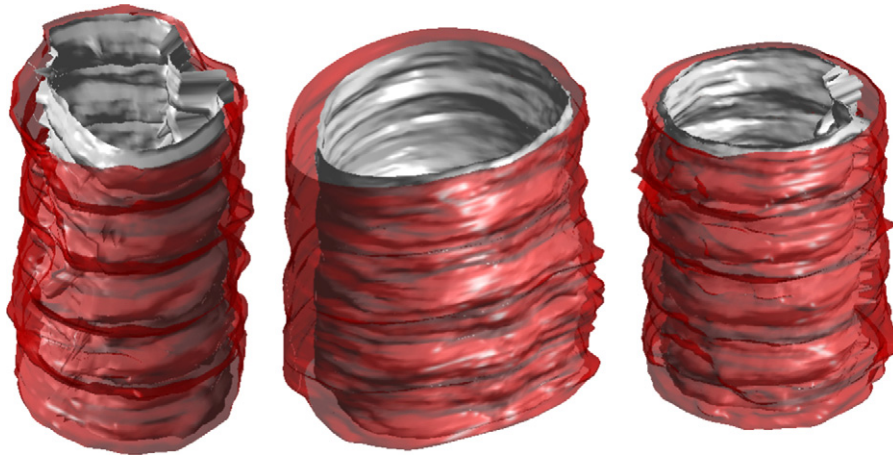


Fig. 9. Three-dimensional reconstructions of 2 mm longitudinal sections for different vessels. In red is shown the media–adventitia contour, in white the lumen contour.

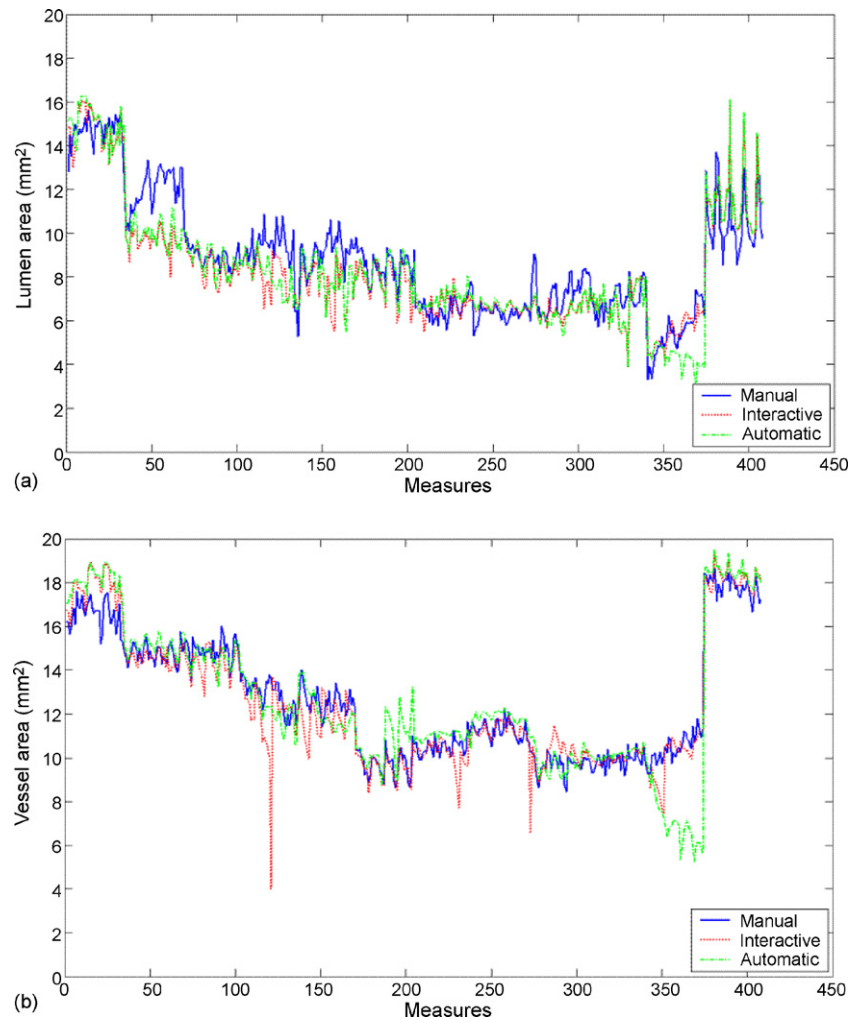


Fig. 10. (a) Plot of lumen area results comparing manual, interactive and automatic methods. (b) Plot of vessel area results comparing manual, interactive and automatic methods. Mismatch in the results between manual (blue) and interactive (red) or automatic (green) methods may be caused by catheter movement or zones of shadow caused by calcified plaque which lead the contour to undesirable regions. This causes the underestimate/overestimate of vessel area, lumen area and amount of plaque. While for lumen area calculus both interactive and automatic methods produce similar results, for vessel area calculus they differ a little more because they use the same algorithm for plaque detection, i.e. lumen area calculus, but different strategies for media–adventitia contour detection, i.e. vessel area calculus, as it has been explained above. In the first case, lumen area, the mismatch of results between interactive/automatic and manual is a little greater than in the second case, vessel area, because there are regions, especially when soft plaque is present, where lumen pixels intensity and plaque pixels intensity can be easily confused so that the method produces an overestimate or an underestimate of plaque, i.e. of lumen area.

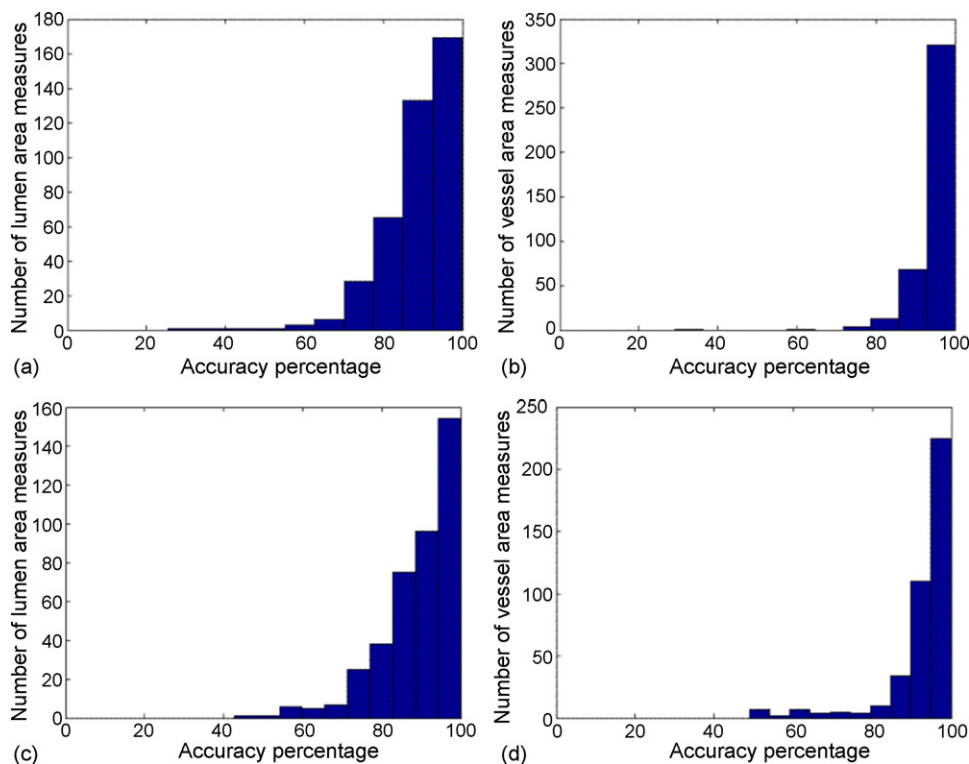


Fig. 11. Histograms of measures accuracy compared to manual results. (a) Lumen area measures for interactive method, (b) vessel area measures for interactive method, (c) lumen area measures for automatic method and (d) vessel area measures for automatic method. The accuracy percentage is the relation between the interactive/automatic measure and the manual one. One can see the interactive method is more accurate than the automatic one as histograms (a) and (b) have more measures in the region of 90–100% of accuracy. In both methods the accuracy is also greater for vessel area measures, because plaque detection, i.e. lumen area calculus, may be mistaken when there's soft plaque, as this can be easily confused with lumen.

sity of the pixels belonging to the plaque region is much higher than that of the pixels belonging to the lumen (see Fig. 7). However, this difference is not so easy to detect when plaque is soft because in this case the pixels intensity is much lower than in calcified plaques and sometimes it is even comparable to the intensity of lumen pixels. When this occurs our method may introduce a small error (see Table 1).

Due to the presence of multiple reflections and the inhomogeneity of blood texture there may be many high intensity pixels “floating” in the lumen. To prevent these pixels from being interpreted as plaque pixels a knowledge based strategy was proposed consisting in the fact that plaque is always attached to the media–adventitia contour. Only those pixels attached to or near the media–adventitia contour were chosen as plaque pixels, while the rest of pixels were discarded as distant or “floating” pixels. Linearly interpolating the inner plaque pixels the lumen contour could be finally determined. Fig. 8 shows the whole process of lumen border detection.

A first estimate of plaque type can be provided taking into account the average intensity of the pixels which form the plaque. Although there are several types of plaque and some of them present similar levels of pixel intensity, our method proved to be accurate in discriminating between soft and calcified plaque where the difference between pixel intensities is quite substantial. Table 3 shows the amount of frames where our expert observer detected soft plaque or calcified plaque. The

amount of error shows that our method matched the observer's choice in most cases.

#### 2.4. Three-dimensional reconstruction

After all the internal and external contours have been detected a three-dimensional reconstruction can be created, as can be observed in Fig. 9. From this 3D reconstruction, all the desired measures of length, area and volume of plaques can be calculated.

### 3. Results

First results are promising and they demonstrate the method accuracy in determining lumen and plaque area and stenosis percentages from the previously detected contours, finding regions where this area presents critical values, calculus of plaque volume and first estimate of plaque type. Media–adventitia contour detection depends highly on the quality of the images so a better reconstruction and a more accurate set of results depend directly on the strategy followed for the contour detection, interactive (requires more user attention) or automatic (possibility of mismatch in the results).

A total number of twelve sequences of thirty-four IVUS frames per sequence were studied from five different patients. The amount of measures to be compared was 12 sequences  $\times$  34 images/sequence = 408 images. On each image six different

Table 2  
Lumen and plaque volume results

Sequence	Manual method		Interactive method		Automatic method	
	Lumen volume (mm <sup>3</sup> )	Plaque volume (mm <sup>3</sup> )	Lumen volume (mm <sup>3</sup> )	Plaque volume (mm <sup>3</sup> )	Lumen volume (mm <sup>3</sup> )	Plaque volume (mm <sup>3</sup> )
1	9.95	1.3	10.03	2.04	10.19	2.12
2	8.18	1.84	6.57	3.3	6.78	3.48
3	6.08	4.07	5.79	3.99	5.97	4.02
4	6.22	2.55	5.47	2.64	5.42	3.02
5	6.23	2.35	5.25	2.83	5.42	2.85
6	5.74	0.85	5.35	1.16	5.58	1.68
7	4.48	2.68	4.55	2.39	4.77	2.7
8	4.29	3.38	4.47	3.19	4.53	3.54
9	4.95	1.65	4.4	2.43	4.34	2.34
10	4.75	1.97	4.61	2.22	4.63	2.3
11	3.7	3.4	3.74	3.06	2.93	1.9
12	7.13	4.98	7.77	4.58	7.83	4.72
Average error	0	0	±0.48 (8%)	±0.45 (17.4%)	±0.52 (8.7%)	±0.61 (23.4%)

It can be seen that the interactive method produces slightly better results for volume calculus but it is clearly slower and it requires continuous action from the user.

Table 3

Plaque estimate results comparing the proposed method (both interactive and automatic methods produce the same results, as they use the same plaque detection algorithm) and the manual method, where experienced observers determined plaque type separately

Manual method (%)			Proposed method (%)	Mismatch between methods (%)
Observation 1	Observation 2	Variability		
Percentage of frames with soft plaque			100	<10
98.33	94.5	<4		
Percentage of frames with hard or calcified plaque			73.25	<10
80.83	83.49	<4		

It shows the percentage of frames with soft or calcified plaque out of the whole set of studied frames. Our method always detected soft plaque (overestimation) as it can be easily confused with intima thickening or lumen, while it underestimated the presence of calcified plaque due to the relatively low intensity of some calcified plaques, which our method ignored.

measures were calculated using three different methods: manual lumen area, interactive lumen area, automatic lumen area, manual vessel area, interactive vessel area and automatic vessel area, summing up a total amount of 2448 measures.

Results show the accuracy of our methods in calculating lumen area, vessel area, lumen volume, plaque volume and plaque type estimate. For the interactive method both a correlation condition of less than 0.94 and periodical pauses were used to stop the process every 20 frames approximately to introduce new contours manually. The automatic method, not needing any manual interaction at all but just the first one in the first frame, proved to be much slower to achieve the results shown here, as it required many more iterations.

To evaluate the accuracy of our method we compared automatic measures of area, volume and plaque estimate to those taken manually by experienced observers.

Area results are shown in Table 1. Percentage accuracy refers to the relation between the interactive/automatic measure and the manual one, while the error is the difference between the interactive/automatic measure and the manual one. Only average results are shown to simplify. Fig. 10 shows the whole set of area measures, comparing the manual, interactive and automatic methods for both lumen and vessel areas. Histograms with the percentage accuracy values are shown in Fig. 11.

To compare volume measures we calculated plaque and lumen volume for each of the twelve IVUS sequences. Values of manual, interactive and automatic methods are shown in Table 2 with their average errors.

Finally the accuracy of our automatic first plaque type estimation method was investigated. Table 3 shows the percentages of the total amount of analysed frames where soft or calcified plaque was detected, comparing those taken manually to those generated automatically. Error determines the percentage of frames in which there was a mismatch.

#### 4. Conclusions and future investigations

The developed method can be used to provide a preliminary analysis of vessel pathologies using a semi-automatic three-dimensional reconstruction of blood vessels from IVUS video sequences. Ideally only an initial contour for the media–adventitia border in the first video frame needs to be provided so that this initial contour is automatically adapted to the following video frames. Then lumen border is detected and finally the three-dimensional reconstruction can be made.

The three-dimensional reconstruction allows to take measures of length, area and volume and thus detect automatically the most problematic regions. It also provides measures of ves-

sel stenosis and first estimate of plaque type. Results show the accuracy of our method in calculating and detecting the mentioned parameters, obtaining an average error of less than  $1 \text{ mm}^2$  in calculating lumen and vessel area measures, equivalent approximately to 10% of the total area for the average manual area measure. For volume calculus the error was smaller than  $0.5 \text{ mm}^3$  both for lumen and plaque, which was equivalent approximately to 10–20% of the total volume for the average manual volume measure. For plaque type estimate the error on soft plaque estimate was less than 2% while it was less than 10% for hard plaque (fibrous and calcified) estimate, providing a very good preliminary evaluation of vessel pathologies from a semi-automatic three-dimensional reconstruction method of blood vessels.

Future investigations will be focused on improving the algorithms speed and on new possible methods to overcome the IVUS video intrinsic problems (such as catheter movement and ultrasonic image noise) as well as on a more complete method to estimate plaque type [14].

## References

- [1] Lee JT, White RA. Basics of intravascular ultrasound: an essential tool for the endovascular surgeon. *Sem Vasc Surg* 2004;17(2):110–8.
  - [2] Klingensmith JD, Shekhar R, Vince DG. Evaluation of three-dimensional segmentation algorithms for the identification of luminal and medial–adventitia borders in intravascular ultrasound images. *IEEE Trans Med Imaging* 2000;19(10).
  - [3] Rotger D, Radeva P, Cañero C, Villanueva JJ. Corresponding IVUS and angiogram image data. In: *IEEE Proc Comput Cardiol*. 2001.
  - [4] Wahle A, Prause GPM, DeJong SC, Sonka M. Geometrically correct 3-d reconstruction of intravascular ultrasound images by fusion with biplane angiography—methods and validation. *IEEE Trans Med Imaging* 1999;18(8).
  - [5] Gil D, Radeva P, Saludes J, Mauri J. Automatic segmentation of artery wall in coronary IVUS images: a probabilistic approach. In: *IEEE Proc Comput Cardiol*. 2000. p. 687–90.
  - [6] Luo Z, Wang Y, Wang W. Estimating coronary artery lumen area with optimization-based contour detection. *IEEE Trans Med Imaging* 2003;22(4).
  - [7] Sonka M, Zhang X, Siebes M, Bissing MS, DeJong SC, Collins SM, McKay CR. Segmentation of intravascular ultrasound images: a knowledge-based approach. *IEEE Trans Med Imaging* 1995;14(4).
  - [8] Plissiti ME, Fotiadis DI, Michalis LK, Bozios GE. An automated method for lumen and media–adventitia border detection in a sequence of IVUS Frames. *IEEE Trans Inform Technol Biomed* 2004;8(2).
  - [9] Xu C, Prince JL. Snakes, shapes and gradient vector flow. *IEEE Trans Image Process* 1998;7(3).
  - [10] Zhu H, Liang Y, Friedman MH. IVUS image segmentation based on contrast, medical imaging 2002: image processing. In: Sonka M, Fitzpatrick JM, editors. *Proceedings of the SPIE*, vol 4684. 2002.
  - [11] Perona P, Malik J. Scale-space and edge detection using anisotropic diffusion. *IEEE Trans Pattern Anal Mach Intell* 1990;12(7).
  - [12] Kass M, Witkin A, Terzopoulos D. Snakes: active contour models. *Int J Comput Vis* 1988;1:32–31.
  - [13] Jain AK. *Fundamentals of digital image processing*. Englewood Cliffs, NJ: Prentice-Hall; 1989.
  - [14] Zhang X, McKay CR, Sonka M. Tissue characterization in intravascular ultrasound. *IEEE Trans Med Imaging* 1998;17(6).
- Roberto Sanz-Requena** was born in Valencia, Spain, in 1981. He received the MSc degree in Telecommunications Engineering from the Universitat Politècnica de València in 2005. He is currently working in Valencia towards his PhD degree in computer science and biomedical technology both at the Universitat Politècnica and at the Quirón Hospital. His research interests are computer sciences applied to medical imaging.
- David Moratal-Pérez** was born in Gandia, Spain in 1976. He received his MSc (2001) and PhD (2006) degrees in Telecommunications Engineering from the Universitat Politècnica de València, Spain. He is also Ingénieur Supélec, 2001, from the École Supérieure d'Électricité, France. Since 2004 he works in the Universitat Politècnica de València as an assistant professor of Electronics and Medical Imaging. His primary research interests concern biomedical imaging and biological signal processing. He works on acceleration strategies in cardiac MRI, collaborating with the Emory University School of Medicine, Atlanta, USA, and he has been also collaborating for clinical validations and medical applications with the Cardiology and Radiology Departments of the Hospital Quirón, Hospital Clínic Universitari and Hospital Universitario Dr. Peset of Valencia, Spain.
- Diego R. García-Sánchez** received the MSc degree in Telecommunications Engineering from the Universitat Politècnica de València in 2003, with an End of Studies Project related to the automatic quantification of myocardial viability in magnetic resonance imaging, developed in collaboration with the Cardiology Department of the Hospital Clínic Universitari of Valencia, where he worked until the first half of 2005 in the development of software tools to assess myocardial viability by multimodality cardiac medical image processing. He worked in Accenture in the Health Information Systems and Technology area until the second half of 2006, when he joined Medtronic as Technical Consultant in Neurostimulation and NeuroNavigation Systems.
- Vicente Bodí** was born in Valencia, Spain, in 1966. He received the MD degree from the Universitat de València in 1990. In 1998 he finished his MD thesis in cardiology. He is currently working as a cardiologist at the Hemodynamics Service of the Hospital Clínic Universitari of Valencia. His research interests include cardiac magnetic resonance imaging, interventional cardiology, myocardial recovery after infarction and bioengineering.
- José Joaquín Rieta** belongs to the official lecturer staff of the Electronic Engineering Department in the Universitat Politècnica de València, developing his teaching responsibilities since 1994 at the Gandía Higher School of Technology. He received the MEng degree in image and sound from the Universidad Politécnica de Madrid in 1991, the MSc degree in Telecommunications from the Universitat Politècnica de València in 1996, and the PhD degree in Biomedical Signal Processing in 2003 in the same University. As lecturer he has imparted several subjects related to Electronic and Biomedical Instrumentation, Analog Systems, Data Conversion Systems and Control Engineering, and has been the author of several docent publications in these areas. He coordinates the Biomedical Synergy research group in the Valencia University of Technology, where is the responsible of the advanced biomedical signal processing research line. His research interests include statistical, non-linear and array signal processing applied to biomedical signals, specially focused in cardiac signals, blind signal separation techniques and the develop of clinical applications to study and characterize the atrial activity inside the challenging problem of supraventricular arrhythmias.
- Juan M. Sanchis** was born in Alcoi (Spain) in 1968. He obtained his MSc (1994) and PhD (2004) degrees in Telecommunications Engineering from the Universitat Politècnica de València. Since October 1994, he has been appointed at the UPV to lead research and teaching in the field of Electroacoustics, and in particular, he teaches sound design in the MA in Audiovisual Communications and Sound Systems in Electrical Engineering. He is involved in research activities in the areas of audio signal processing (blind separation performance of acoustic mixtures) and medical signal processing (ICA & BSS in biomedical signals). He is a member of AES.